# Chapter 6

## Amino Borate-Functionalized Reduced Graphene Oxide Further Functionalized with copper Phthalocyanine Nanotubes for Reducing Friction and Wear

The nucleophilic substitution occurs in graphene at the epoxy groups by the attack of ionic liquids, amines, amino acids, small molecular weight polymers, and silane compounds [(Kuila et al. (2012), Gan et al. (2019), Song et al. (2017)]. In the present investigation, therefore, 2-aminoethyl diphenyl borate (ADB) has been willfully picked for nucleophilic attack of the amino group at the epoxide rings of GO forming ADB-rGO. Use of ADB has been favored to surmount the advantages of boron-nitrogen synergy for *in situ* formation of boron nitride (BN) in the tribofilm during tribo-test [Jaiswal et al. (2104), Li et al. (2014), Qiao et al. (2003), Yan et al. (2014), Li et al. (2015)]. The GO was itself reduced to rGO during functionalization. For improvement of triboactivity, some other tribo-active material may be used for non-covalent functionalization of ADB-rGO. In non-covalent functionalization, molecules undergo physical adsorption on the surface of graphene via the weaker type of interactions such as electrostatic, π-π, or van der Waals forces [Kuila et al. (2012)]. Various conjugated polymers and aromatic compounds are reported to stabilize graphene structure in the composite materials through π-π interactions [Kuila et al. (2012), Georgakilas et al. (2012), Haruna et al. (2019)].

Phthalocyanine (Pc), a sixteen membered macrocyclic ligand, is composed of four isoindole units linked together by nitrogen atoms. It has two-dimensional geometry possessing a conjugated system of eighteen π-electrons that provide remarkable thermo-oxidative stability [Gregory et al. (2012), Moussaron et al. (2013)]. Phthalocyanine owing to extensive

conjugation, has numerous applications in various technological fields [Gregory et al. (2012), Moussaron et al. (2013), Koyun et al. (2019)]. The role of the π-electron system is of utmost significance in charge-carrier transport-related properties, while the planar structure renders importance in the field of lubrication [Tewari et al. (1989), Nader et al. (1991), Nader et al. (1992)]. Metal complexes resulting from deprotonation of phthalocyanine ligand; have been acknowledged in emerging areas of research [Zhang et al. (2011), García-Iglesias et al. (2011), Mohammed et al. (2019)] including lubrication [Tewari et al. (1989)].

Chunder and his associates prepared a composite of reduced graphene oxide with tetrasulfonate salt of copper phthalocyanine to accomplish the cumulative effect of phthalocyanine and graphene. They studied its optoelectrical properties [Chunder et al. (2010)]. Zinc phthalocyanines have been used as electron donors for surface modification of graphene, and the resulting composite is applied as electrode material in solar cells [Kuila et al. (2012)]. It is well known from the papers published in this area that adsorption of the additive has a dominating effect on tribo-activity [Kavita et al. (2020), Jaiswal et al. (2014), fetLi et al. (2014), Qiao et al. (2003), Yan et al. (2014), Li et al. (2015), Kumar et al. (2019)]. The importance of phthalocyanines triggered us to carry out a detailed classical molecular dynamics (MD) investigation of the adsorption of phthalocyanine and copper (II) phthalocyanine on the steel surface in paraffin oil. Classical MD simulations are capable of investigating the molecular aspects of adsorption of Pc and CuPc to the Fe surface in the presence of PO molecules [Kumar et al. (2019), Kuntail et al. (2019), Jain et al. (2019)]. The

MD investigation predicted that CuPc adsorbs better than Pc on the steel surface and also has a tendency to flip between folded and unfolded conformations. Following this, the nanotubes (NTs) of CuPc were prepared and characterized. The tribological properties of CuPc nanotubes were found to be remarkably better than Pc. Nanotube (NT) morphology is well known to produce excellent tribological results, mainly in the boundary lubrication regime [Khalil et al. (2016), Salah et al. (2017)]. The carbon nanotubes (CNTs) have been extensively studied for their high level of antiwear efficiency and load caring capacity [Khalil et al. (2016), Salah et al. (2017), Zhang et al. (2015)]. Chattopadhyay and co-workers have investigated the photocatalytic activity of graphene wrapped copper-phthalocyanine nanotubes for industrial wastewater treatment [Mukherjee et al. (2017), Samanta et al. (2018)]. Moreover, nanosheets, in general, provide excellent tribological properties due to the feasibility of sliding of one sheet over the other due to weak van der Waals forces existing between them. Accordingly, the composite $MoS_2$-rGO has shown exalted activity [Verma et al. (2020)]. Since CuPc also possesses a layered structure, for the enhancement of tribo-activity of the layered structure of ADB-rGO, CuPc NTs were used to form CuPc-(ADB-rGO) anticipating tribological activity of high order. Tribological properties of Pc, CuPc nanotubes, GO, ADB-rGO and CuPc-(ADB-rGO) were, therefore, evaluated in paraffin oil using ASTM D4172 and ASTM D5183 tests employing a four-ball tester.

### 6.1. Molecular Dynamics Simulation Studies

Molecular dynamics (MD) investigations were carried out on two model systems. One, which considers the adsorption of a phthalocyanine (Pc) molecule, and the other that studies copper

phthalocyanine (CuPc)) on Fe (110) surface in the presence of paraffin oil (PO). A collection of 20 straight-chain alkane molecules ($C_{18}H_{38}$) modelled the PO. Materials and Processes Simulations Platform (MAPS version 4.0.1 from Scienomics SARL Paris, France) was used to construct the two models: 1Pc/20PO/Fe(110) and 1CuPc/20PO/Fe(110), respectively. The production run data of the MD simulations were used to calculate the adsorption energies and long-time average radial distribution functions (RDF).

### 6.1.1. Computational Model Construction

Modified Neglect of Diatomic Overlap (MNDO), a semi-empirical method, optimized the geometry of molecules in the simulation. The starting point was a model consisting of a BCC rectangular slab (of 44.39Å×42.90Å×12.5Å size) containing 1815 Fe atoms occupying one side of a simulation box of dimensions 44.39Å×42.90Å× 81.05Å. The (110) surface of the Fe slab was perpendicular to the z-axis of the simulation box. **Fig. 6.1a** shows this empty slab model. The space in the z-direction of the system after the Fe slab is called the vacuum gap. It was necessary to include this vacuum to remove the interactions between periodic images in the z-direction.

The next stage involved the insertion of one solute (Pc or CuPc) and 20 $C_{18}H_{38}$ molecules (making the PO solvent) on top of the Fe (110) surface. The polymer consistent force field (PCFF) took care of all interactions in this model. Additional parameters necessary for simulation of CuPc adsorption to the Fe slab were incorporated into the PCFF interaction potential expression from reference. **Equation 6.1** gives the 9-6 Lennard Jones (LJ) pair

potential [Shao et al. (2014), Sun et al. (1994)] that models the non-bonded van der Waal (iron surface/adsorbate/ solvent molecules) interaction part of this force field.

$$\mathbf{E}_{LJ} = \varepsilon[\,\mathbf{2}\left(\frac{\sigma}{r_{min}}\right)^{\mathbf{9}} - \mathbf{3}\left(\frac{\sigma}{r_{min}}\right)^{\mathbf{6}}] \quad \text{.....} \qquad 6.1$$

In this expression, ε denotes the well-depth, σ is the van der Waals radii, and the distance between any two atom types is $\boldsymbol{r_{min}}$. In this expression, ε denotes the well-depth, σ is the van der Waals radii, and the distance between any two atom types is $\boldsymbol{r_{min}}$.

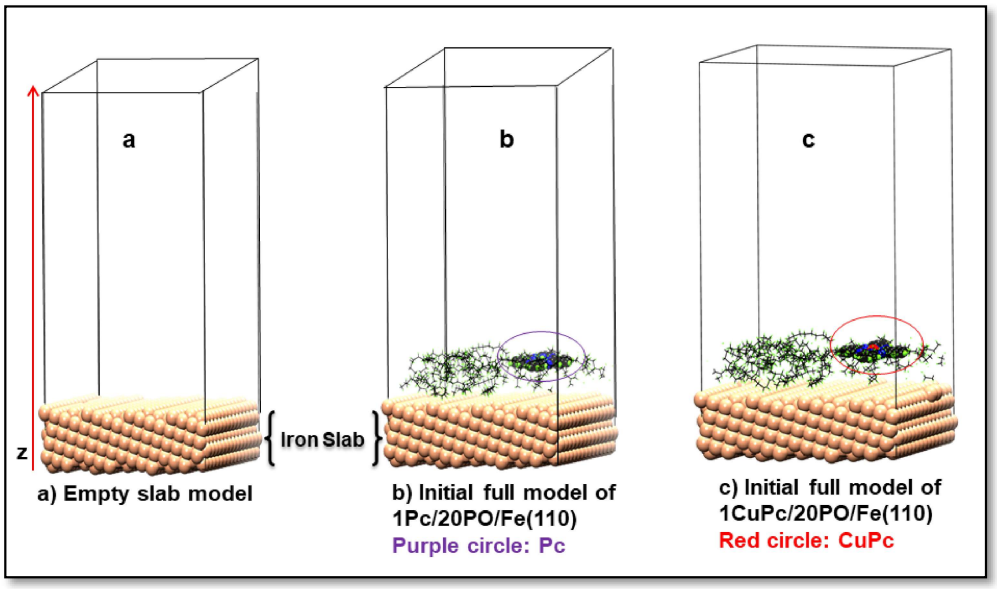


**Fig. 6.1.** (a) Empty slab model (b) initial model of the full system with 1Pc and 20 PO molecules on the Fe surface, (c) initial model of the full system with 1 CuPc and 20 PO molecules on top of the Fe slab.

**Table 6.1** of supporting information gives all PCFF pair-wise potential (bonded and non-bonded) parameters used in these simulations. **Fig. 6.1b** shows the picture of the initial system after the insertion of one Pc and 20 PO molecules on top of the Fe slab. Similarly, **Fig. 6.1c** depicts the image of the complete initial system after the insertion of one CuPc and 20 PO molecules adjacent to the Fe slab.

**Table 6.1**. Detailed PCFF potential parameters for the different pairwise interactions possible between the Fe surface and different atom types in PO, Pc, and CuPc adsorbate molecules.

PCFF Non-Bonded LJ Interaction Potential formula:

$$\mathbf{E_{LJ}} = \in_{\mathbf{0}} \left[ \mathbf{2}\left(\frac{\boldsymbol{\sigma}}{r_{min}}\right)^{\mathbf{9}} - \mathbf{3}\left(\frac{\boldsymbol{\sigma}}{r_{min}}\right)^{\mathbf{6}} \right] \quad \text{….. …….. ……6.2}$$

| I | $\in_0$ (kcal/mol) | σ (Å) |
|---|---|---|
| Fec | 0.820 | 4.22 |
| Feh | 0.193 | 3.02 |
| Cu | 3.818 | 2.67 |
| NH | 0.134 | 4.7 |
| Fe | 13.889 | 2.65 |
| N2 | 0.120 | 3.40 |
| C2 | 0.068 | 3.91 |
| H | 0.023 | 2.87 |
| c | 0.054 | 4.01 |
| h | 0.020 | 2.99 |
| CR | 0.064 | 4.01 |

Quartic bond Formula: $\mathbf{E}_{bond} = \boldsymbol{k_2}(\boldsymbol{r}-\boldsymbol{r_0})^2 + \boldsymbol{k_3}(\boldsymbol{r}-\boldsymbol{r_0})^3 + \boldsymbol{k_4}(\boldsymbol{r}-\boldsymbol{r_0})^4$ …… 6.3

| I | J | $k_2$ (kCal/mol*Å$^{-2}$) | $r_0$ (Å) | $k_3$ (kCal/mol*Å$^{-3}$) | $k_4$ (kCal/mol*Å$^{-4}$) |
|---|---|---|---|---|---|
| Cu | N2 | 245.000000 | 1.954000 | -88.919300 | 55.417400 |
| C2 | H | 372.825100 | 1.098200 | -803.452600 | 894.317300 |
| C2 | C2 | 470.836100 | 1.417000 | -627.617900 | 1327.634500 |
| C2 | N2 | 325.343300 | 1.375000 | −204.408200 | 466.398900 |
| C2 | NH | 477.520200 | 1.374900 | -848.559200 | 1022.390900 |
| H | NH | 463.923000 | 1.005300 | -1050.807000 | 1284.726200 |
| c | c | 299.670000 | 1.530000 | -501.770000 | 679.810000 |
| c | h | 345.000000 | 1.101000 | -691.890000 | 844.600000 |
| CR | CR | 844.600000 | 1.417000 | -627.617900 | 1327.634500 |
| CR | H | 372.825100 | 1.098200 | -803.452600 | 894.317300 |

Quartic angle Formula: $\mathbf{E}_{\theta} = \boldsymbol{k_2}(\theta-\theta_0)^2 + \boldsymbol{k_3}(\theta-\theta_0)^3 + \boldsymbol{k_4}(\theta-\theta_0)^4$ ……..6.4

| I | J | k | $k_2$ (kCal/mol*deg$^{-2}$) | $\theta_0$ (deg) | $k_3$ (kCal/mol*deg$^{-3}$) | $k_4$ (kCal/mol*deg$^{-4}$) |
|---|---|---|---|---|---|---|
| C2 | N2 | Cu | 49.820300 | 125.880000 | -13.475000 | 5.857000 |
| N2 | Cu | N2 | 59.574100 | 90.000000 | -35.254500 | 16.051700 |
| C2 | C2 | H | 35.155800 | 117.940000 | 12.468200 | 0.000000 |
| C2 | C2 | C2 | 61.022600 | 118.900000 | 34.993100 | 0.000000 |
| C2 | C2 | N2 | 74.247400 | 122.855000 | −50.000000 | 0.000000 |
| N2 | C2 | N2 | 90.523000 | 127.6575 | −20.801000 | −18.0000 |
| C2 | N2 | H | 48.232000 | 115.5720 | −5.798000 | −9.966000 |
| C2 | NH | H | 109.774600 | 106.010000 | -9.063600 | 0.000000 |
| NH | C2 | N2 | 98.851900 | 108.910000 | -5.750200 | 0.000000 |
| C2 | NH | H | 47.012000 | 109.380000 | -17.355600 | 0.000000 |
| H | C2 | NH | 43.840800 | 109.800000 | -9.515300 | 0.000000 |
| H | C2 | N2 | 40.827500 | 110.550000 | -13.031800 | 0.000000 |
| C2 | C2 | NH | 78.641800 | 112.590000 | -16.388800 | 0.000000 |
| c | c | c | 39.516000 | 112.670000 | -7.443000 | -9.558300 |
| c | c | h | 41.453000 | 110.770000 | -10.604000 | 5.129000 |
| CR | CR | H | 35.155800 | 117.940000 | 12.468200 | 0.000000 |
| CR | CR | CR | 61.022600 | 118.900000 | 34.993100 | 0.000000 |

Torsion Formula:

$$\mathbf{E}_{\emptyset} = \boldsymbol{k_2}[\mathbf{1} - \boldsymbol{cos}(\emptyset + \emptyset_1)] + \boldsymbol{k_3}[\mathbf{1} - \boldsymbol{cos}(2\emptyset + \emptyset_2)] + \boldsymbol{k_3}[\mathbf{1} - \boldsymbol{cos}(3\emptyset + \emptyset_3)] \quad \ldots. \mathbf{6.5}$$

| I | J | K | L | $k_1$ (kCal/mol) | $\Phi_1$ (deg) | $k_2$ (kCal/mol) | $\Phi_2$ (deg) | $k_3$ (kCal/mol) | $\Phi_3$ (deg) |
|---|---|---|---|---|---|---|---|---|---|
| C2 | C2 | N2 | Cu | 1.840500 | 0.000000 | 5.477900 | 0.000000 | 3.140700 | 0.000000 |
| C2 | N2 | Cu | N2 | -6.956400 | 0.000000 | 17.730900 | 0.000000 | -5.050800 | 0.000000 |
| N2 | C2 | N2 | Cu | -3.954500 | 0.000000 | 4.886400 | 0.000000 | 0.000000 | 0.000000 |
| C2 | C2 | C2 | C2 | 8.366700 | 0.000000 | 1.200000 | 0.000000 | 0.000000 | 0.000000 |
| H | C2 | C2 | H | 0.000000 | 0.000000 | 2.350000 | 0.000000 | 0.000000 | 0.000000 |
| C2 | C2 | C2 | CR | 0.000000 | 0.000000 | 3.966100 | 0.000000 | 0.000000 | 0.000000 |
| N2 | C2 | C2 | C2 | 3.195200 | 0.000000 | 11.274500 | 0.000000 | −1.445600 | 0.000000 |
| C2 | C2 | N2 | C2 | 0.000000 | 0.000000 | 1.000000 | 0.000000 | 0.000000 | 0.000000 |
| N2 | C2 | N2 | C2 | 0.000000 | 0.000000 | 1.000000 | 0.000000 | 0.000000 | 0.000000 |
| C2 | C2 | C2 | NH | 11.527000 | 0.000000 | 2.718300 | 0.000000 | 0.000000 | 0.000000 |
| C2 | C2 | NH | C2 | 10.876500 | 0.000000 | 6.347500 | 0.000000 | 0.000000 | 0.000000 |
| C2 | C2 | NH | H | 0.000000 | 0.000000 | 1.820200 | 0.000000 | 0.000000 | 0.000000 |
| NH | C2 | N2 | C2 | 0.000000 | 0.000000 | 9.783000 | 0.000000 | 0.000000 | 0.000000 |
| N2 | C2 | NH | C2 | 0.000000 | 0.000000 | 20.017300 | 0.000000 | 0.000000 | 0.000000 |
| N2 | C2 | NH | H | 0.000000 | 0.000000 | 3.509600 | 0.000000 | 0.000000 | 0.000000 |
| c | c | c | c | 0.000000 | 0.000000 | 0.051400 | 0.000000 | -0.143000 | 0.000000 |
| c | c | c | h | 0.000000 | 0.000000 | 0.031600 | 0.000000 | -0.168100 | 0.000000 |
| h | c | c | h | -0.143200 | 0.000000 | 0.061700 | 0.000000 | -0.108300 | 0.000000 |
| CR | CR | CR | CR | 8.366700 | 0.000000 | 1.200000 | 0.000000 | 0.000000 | 0.000000 |
| H | CR | CR | H | 0.000000 | 0.000000 | 2.350000 | 0.000000 | 0.000000 | 0.000000 |

Bond Increment Formula: $\boldsymbol{q_i = \sum \delta_{ij}}$ ..... ..... 6.6

| I | J | $\delta_{ij}$ | $\delta_{ji}$ |
|---|---|---|---|
| C2 | N2 | 0.240500 | -0.240500 |
| Cu | N2 | 0.219100 | 0.000000 |
| C2 | C2 | 0.000000 | 0.000000 |
| C2 | NH | -0.050000 | 0.050000 |
| C2 | H | -0.126800 | 0.126800 |
| NH | NH | 0.000000 | 0.000000 |
| N2 | N2 | 0.000000 | 0.000000 |
| NH | N2 | -0.282300 | 0.282300 |
| c | c | 0.000000 | 0.000000 |
| CR | CR | 0.000000 | 0.000000 |
| CR | C2 | 0.000000 | 0.000000 |
| c | h | -0.053000 | 0.053000 |

### 6.1.2. MD Simulation Details

All three coordinates of the model systems were subject to periodic boundary conditions. The MD simulations were carried out under NVE ensemble constraints, and the particle mesh approach was utilized to implement the long-range Coulomb interaction cut-off at 12 Å distance. The initial temperatures of both systems were 298 K. Large-scale Atomic/Molecular Massively Parallel Simulator (LAMMPS) [Plimpton et al. (1995)]etfet script was applied to run the MD simulations. The total runtime of each MD simulation was 20 nanoseconds with a time step of 1 femtosecond. The first 13 nanoseconds of these runs were used to equilibrate the model systems. The last seven nano-second production run data of the MD simulations were used to calculate the adsorption energies and long-time average radial distribution functions (RDF).

It may be noted that the Fe atoms were not fixed in the slab. The mechanism of interaction between the additive molecule and the steel surface can be reasonably explained from the observed results. In this case, the adsorption energy is the difference between the long-time average (over the production run) of the potential energy of the system with three interacting components (adsorbent, PO, and the additive molecule) ($E_{final}$) and the sum of potential energies of the three reference systems ($E_{Fe110} + E_{1CuPc} + E_{20PO}$). Therefore, the following formula expresses the adsorption energy for the investigated case.

$$E_D = E_{(1CuPc/20PO/Fe\,(110))} - (E_{Fe110} + E_{1CuPc} + E_{20PO}) \quad 6.7$$

## 6.2. Materials and Method

### 6.2.1. Chemicals

Extra pure 2-aminoethyl diphenyl borate, phthalocyanine(Pc), and copper(II) phthalocyanine (CuPc) were supplied by Sigma-Aldrich. The other general chemicals of analytical grade were used.

### 6.2.2. Synthesis of Nanoadditives

#### 6.2.2.1. Preparation of CuPc Nanotubes

CuPc nanotubes were synthesized by the reported method [Mukherjee et al. (2017)]. In a typical experiment, CuPc (0.114g) powder was dispersed in 250 ml chloroform solution, and the solution was ultrasonicated for 30 minutes. The solution was stirred for 6 h after the addition of 4 ml of trifluoroacetic acid ($CF_3COOH$). $CF_3COO^-$ ions interact with the $Cu^{2+}$ ions of CuPc molecules and act as bridging agents for formation of the self-assembled nanotubes [Mukherjee et al. (2017)]. The resulting precipitate was collected and dried for 10 h. The dry powder was dispersed in ethanol and kept at 180 °C for 20 h in a Teflon coated stainless-steel autoclave of 150 ml capacity. After the autoclave reaches slowly the ambient temperature, the appearing precipitate was filtered, washed with ethanol, and dried at 60°C for 8 h yielding CuPc nanotubes.

### 6.2.2.2. Preparation of Borated Amine functionalized rGO (ADB-rGO)

Microwave-assisted modified Hummer's method was used to synthesize graphene oxide (GO) nanosheets [Verma et al. (2019)]. Nucleophilic substitutions at epoxide rings of GO was accomplished by 2-aminoethyl diphenyl borate. Graphene oxide (0.5 g) was dispersed in 100 ml distilled water by ultrasonication for around 1h. The resulting dispersion was centrifuged for about 0.5h. A solution of 2.0 g of 2-aminoethyl diphenyl borate (ADB) in 80 ml ethanol was added to the centrifugate, and the mixture was refluxed for about 24 h. The black product was filtered, washed repeatedly with ethanol and water mixture, and dried at 60 °C [Paul et al. (2016)]. Mechanism of nucleophilic substitution is pictorially depicted in the following scheme-

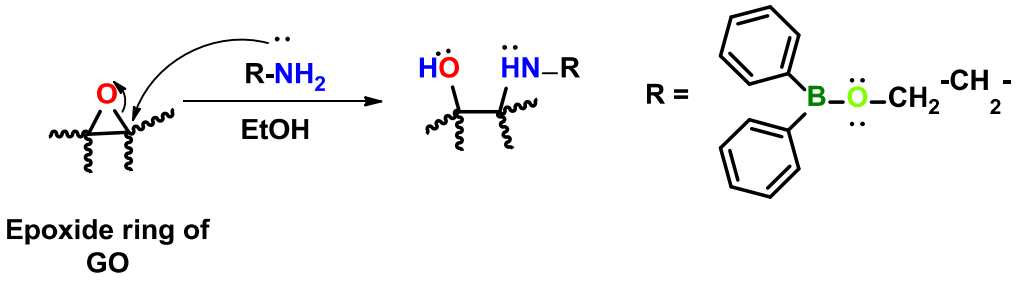


### 6.2.2.3. Preparation of CuPc-(ADB-rGO)

The solutions of CuPc nanotubes and ADB-rGO (0.5 g each in 25 ml DMF) were mixed and stirred for 2h. The mixture was heated at 90 °C for 1 h till the color changes to black. The product was filtered and dried for 6 h to obtain the CuPc-(ADB-rGO) [Mukherjee et al. (2017)].

### 6.3. Sample preparation

For optimization of concentration, series of the admixtures of different additives in paraffin oil was prepared in varied concentrations 0.025, 0.050, 0.075, 0.100, 0.125, and 0.150% w/v through 1 h sonication at room temperature. The antiwear tests were performed for all these admixtures following the test norms imposed by the American Society for Testing and Materials, ASTM D 4172 on Ducom four-ball tester; by this test, the relative wear preventive behavior of lubricating fluids is determined in sliding contact under the *standard test conditions of applied load 392 N, sliding speed 1200 rpm and temperature 75 °C.* The wear scar diameter of the three stationary balls was noted, and their mean has been represented as MWD. The graphs were plotted between concentration and mean wear scar diameter (MWD). Since minimum MWD was found for the concentration of 0.05% w/v, the tribo-activity tests were performed at the same concentration. Besides this, load ramp tests were also conducted following ASTM D5183 standards.

### 6.4. Results and Discussion

#### 6.4.1. The Outcome of the MD Data and RDF Analysis

The adsorption energies of systems involving CuPc and Pc (in PO) on Fe (110) surface show that CuPc has a more negative value of the energy of adsorption(-1650Kcal/mole) than that obtained for Pc (-1605 Kcal/mole), demonstrating that the former adsorbs more strongly than the latter. Therefore, triboactivity of CuPc is expected to be better than Pc.

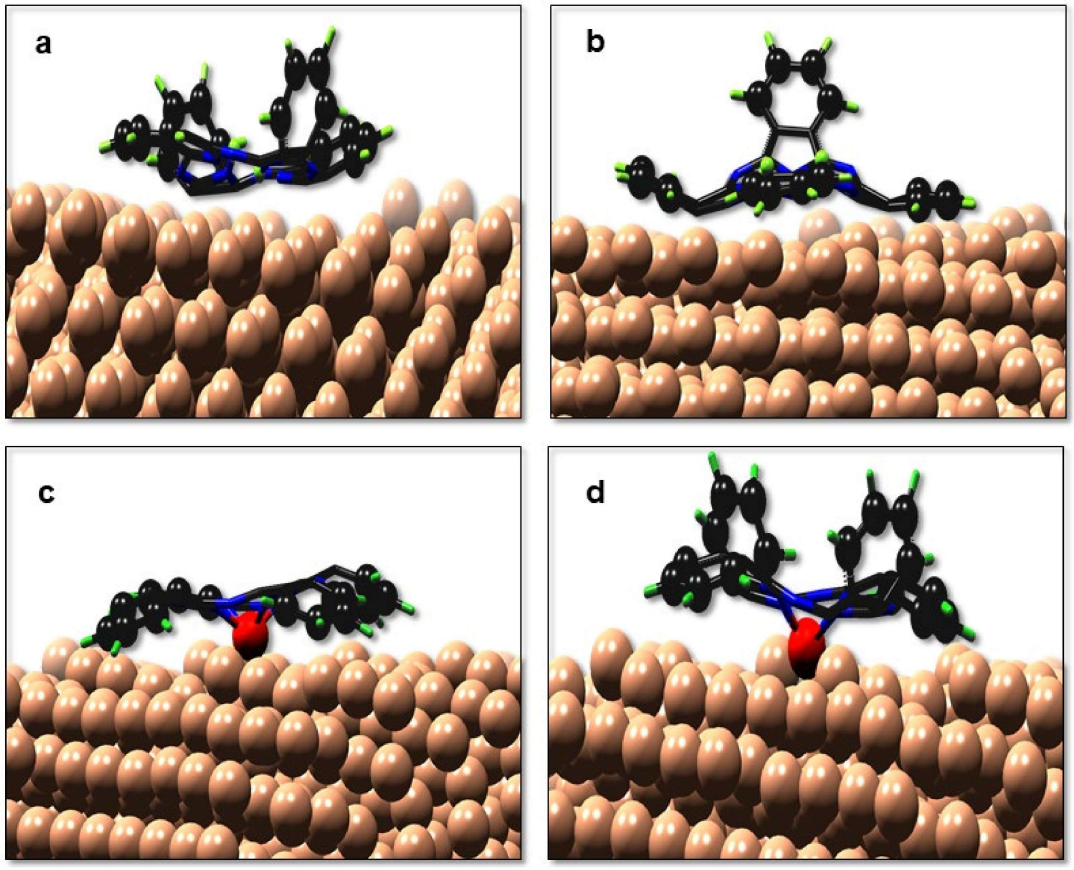


**Fig. 6.2.** (a and b) Snapshots of different conformations of the adsorbate Pc on the Fe(110) surface. (c and d) Snapshots of different configurations of the adsorbate CuPc on the Fe(110) surface. These pictures do not show the PO molecules. Colors representative of different atoms in these pictures are as follows: black, carbon; green, hydrogen; brown, iron; blue, nitrogen; red, copper.

Parts a and b of **Fig. 6.2** display the typical conformations of adsorbed Pc molecule on the Fe (110) surface. It appears that the molecule mainly interacts through the Fe-N linkage. Thus, in **Fig.6.2a**, the outer phenyl rings (part of the isoindole units) seem to get distorted, and two

of them get flipped upwards. In the other arrangement (**Fig. 6.2b**), only one peripheral phenyl ring got flipped upwards, but the rest of them remained near to the Fe (110) surface.

Parts c and d of **Fig. 6.2** show two typical conformations of the CuPc molecule when adsorbed on the Fe (110) surface. The analysis of several frames shows that the system appears to flip or alternate between two conformations. In both arrangements, the CuPc molecule interacts with the Fe slab mainly through the strong Fe-Cu interaction. In one case, **Fig. 6.2c** other parts of CuPc are also parallelly aligned to the Fe slab surface. Another arrangement, **Fig. 6.2d**, maintains the binding of the CuPc molecule through the Fe-Cu linkage, while the two outer phenyl rings move upwards and away from the Fe (110) surface. Thus, CuPc tends to fold /unfold upon adsorption on the steel surface.

Snapshots only give a qualitative view of the problem. Long-time average RDF plots for interactions between different atoms of the adsorbate molecules and Fe provide a quantitative understanding of the phenomena involved [Kumar et al. (2019), Kuntail et al. (2019), Jain et al. (2019)]. Parts a and b of **Fig. 6.3** illustrate the Pc and the CuPc compounds, along with the atom types used in the present MD simulations. These RDF plots are between one atom type in the adsorbate molecule and the Fe atoms making up the slab. But to understand the adsorption of the additive molecule to the adsorbent surface, we only consider the first peak because it gives the probability of finding the concerned atom type (in the additive) at a given distance from the nearest Fe atom.

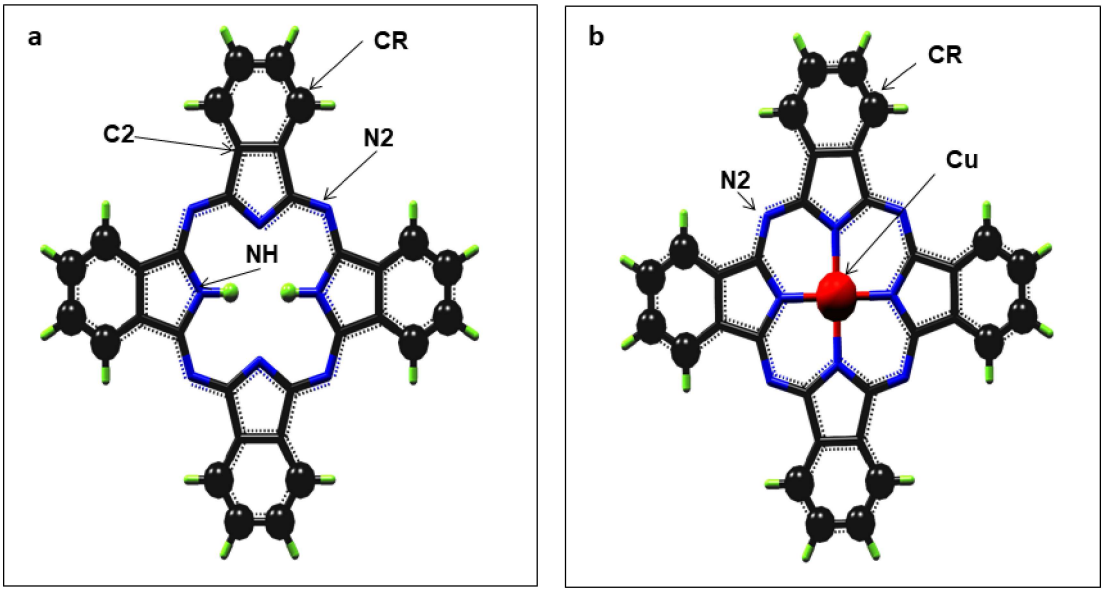


**Fig. 6.3.** (a) Atom type representation in Pc compound and (b) Atom type representation in CuPc compound.

**Fig. 6.4a** gives the RDF plots of different interactions possible between atoms of Pc and the Fe slab. There are two atom types of nitrogen present (N2 and NH) in Pc. The N2 atom type is $sp^2$ hybridized, and the first peak of the r(Fe-N2) linkage occurs around ~3.1Å (the green plot in **Figure 6.4a**. Also, this peak is of higher intensity than those that occur in other RDF plots of Pc. In contrast to this, the NH atom type is $sp^3$ hybridized, and the r(Fe-NH) interaction displays a maximum only after ~ 3.5Å (see the blue plot in **Fig. 3a**).

**Fig. 6.4b** presents RDF plots depicting the interactions between different atoms of CuPc and Fe. The r[(Fe-Cu] plot shows the highest maximum at a distance of 2.5 Å. The maxima of r(Fe–N2, r(Fe-CR), and r(Fe-C2) plots are between 3.0Å to 3.3 Å. Furthermore, the intensity

of the Fe-Cu interaction is also highest, showing that CuPc is mainly attached to the Fe surface through this linkage. Overall, the reason for the enhanced adsorption property of CuPc molecule on Fe slab is the robust Fe-Cu linkage, as illustrated by the RDF plots.

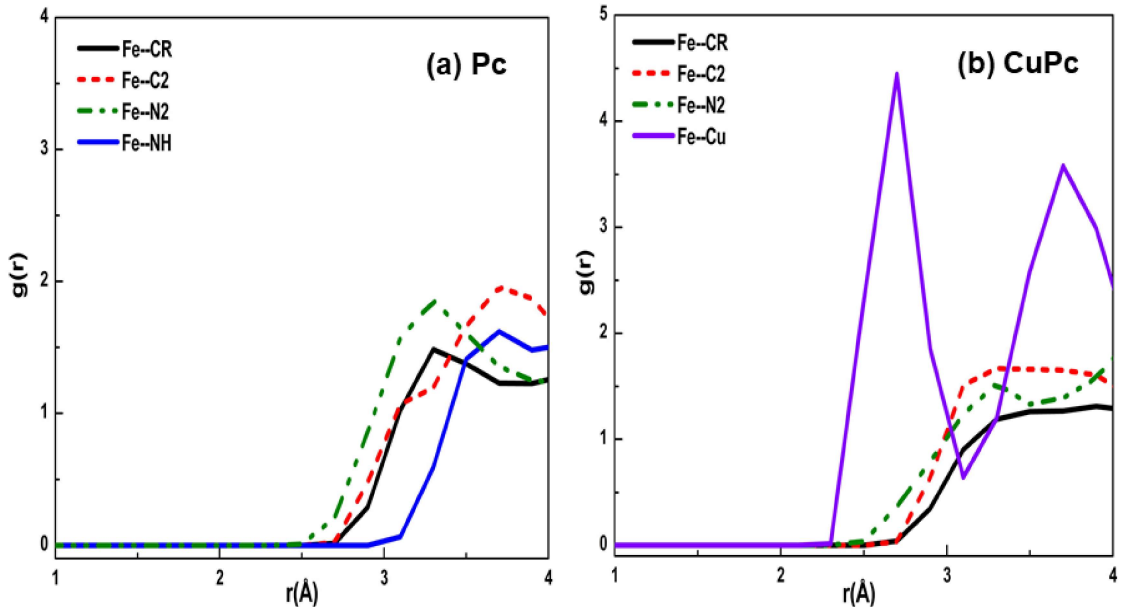


**Fig. 6.4.** Radial distribution functions [g(r)] of the interactions between different atoms of (a) Pc and (b) CuPc molecule with the nearest Fe atom in the slab.

### 6.4.2. Characterization of the Synthesized Additives

The sophisticated techniques, namely XRD, FTIR, UV/visible, Raman, TEM/HR-TEM, and HR-SEM, have been put to use for the characterization of Pc, CuPc NTs, GO, ADB-rGO, and CuPc-(ADB-rGO). XPS has also been used to characterize CuPc-(ADB-rGO). The HR-SEM images of GO nanosheets, functionalized rGO nanosheets ADB-rGO, CuPc nanotubes, and the CuPc-(ADB-rGO) are illustrated in **Fig. 6.5a-e**, respectively. The layered structure

of GO and amino borate functionalized rGO is visible in parts a and b of **Fig. 6.5**, respectively. The EDX spectrum of ADB-rGO given in **Fig. 6.5b$_1$** approves the functionalization of rGO by borated amine based on the presence of additional peaks due to boron and nitrogen. **Fig. 6.5c** reveals nanotube morphology for the copper-phthalocyanine complex [Mukherjee et al. (2017)]. The HR-SEM image of CuPc-(ADB-rGO) manifests the CuPc nanotubes embellishing functionalized reduced graphene oxide. The EDX spectrum, **Fig. 6.5d$_1$** ratifies the functionalization of rGO by ADB and CuPc as all its elements copper, nitrogen, boron, oxygen, are visible along with carbon.

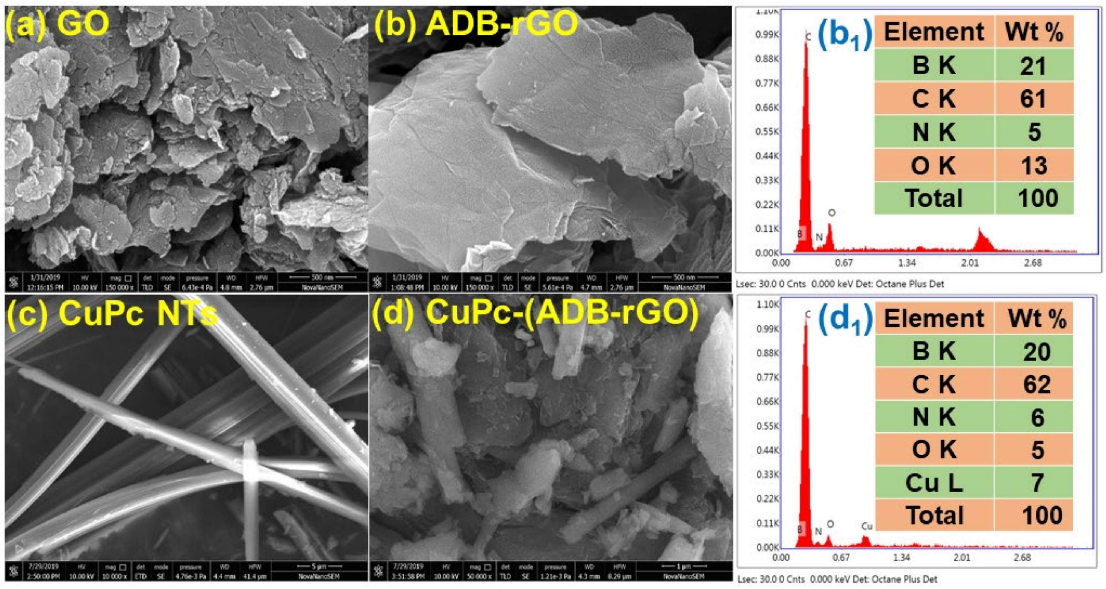


**Fig. 6.5.** HR-SEM images of (a) GO, (b) ADB-rGO, (c) CuPc NTs, and (d) CuPc-(ADB-rGO) and EDX spectra of ($b_1$) ADB-rGO and ($d_1$) CuPc-(ADB-rGO).

The TEM images of GO, ADB-rGO, CuPc nanotubes, and CuPc functionalized rGO, CuPc-(ADB-rGO) are displayed in parts a-d of **Fig. 6.6**, respectively. **Fig. 6.6a** shows rGO

nanosheets folded at the edges while amino borate functionalized graphene nanosheets illustrated in **Fig. 6.6b** look stretched. In HR-TEM images (**Fig. 6.6a$_1$, b$_1$**), the interplanar spacing is increased from 0.341 in GO to 0.346 in ADB-rGO, supporting functionalization by ADB. The hollow nanotube of CuPc having a width around 80-170 nm is perceptible in **Fig. 6.6c**. The TEM image of CuPc-(ADB-rGO), **Figure 6.6d** manifests rGO nanosheets merely wrapped around CuPc nanotubes just by non-covalent interactions [Mukherjee et al. (2017)].

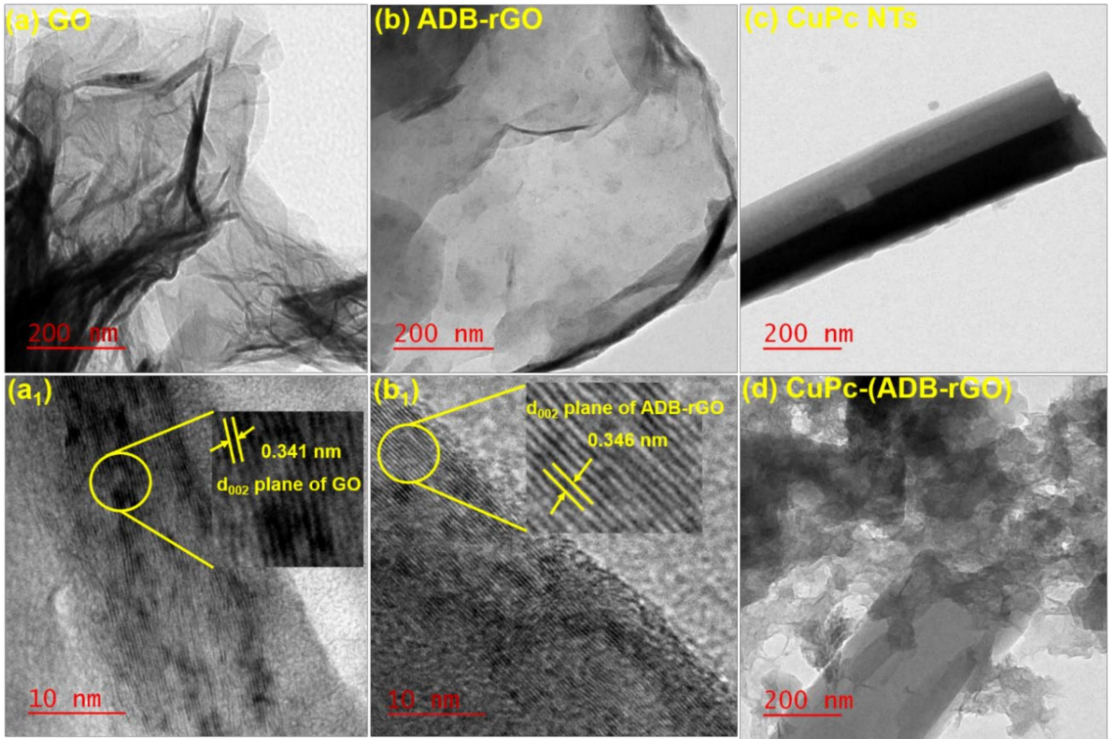


**Fig. 6.6.** TEM images of (a) GO, (b) ADB-rGO, (c) CuPc NTs, and (d) CuPc-(ADB-rGO) and HR-TEM images of ($a_1$) GO and ($b_1$) ADB-rGO.

The XRD patterns of GO, covalently modified rGO by amino borate (ADB-rGO) and further non-covalently modified ADB-rGO by CuPc nanotubes, CuPc-(ADB-rGO) are depicted in **Fig. 6.7**. The characteristic peak of GO falling at 11.8° is conspicuously absent in the case of ADB-rGO, and a new peak becomes noticeable at 25.3°, affirming reduction of GO to form rGO [Mukherjee et al. (2017)]. In the XRD pattern of CuPc NTs, two distinctive strong peaks are perceived at 7 and 9.2 (2-Theta), indicating the formation of β phases. Besides these peaks, few more peaks are also identified at 10.55°, 12.45°, 18.05°, 18.55°, 23.75°, 26.25°, 27.95°, 29.65°, 30.4°. All these peaks are in concurrence with the JCPDS file no. 39-1881. However, there are slight shifts of the peaks in the case of CuPc-(ADB-rGO) [Paul et al. (2019), Mukherjee et al. (2017), Samanta et al. (2018)].

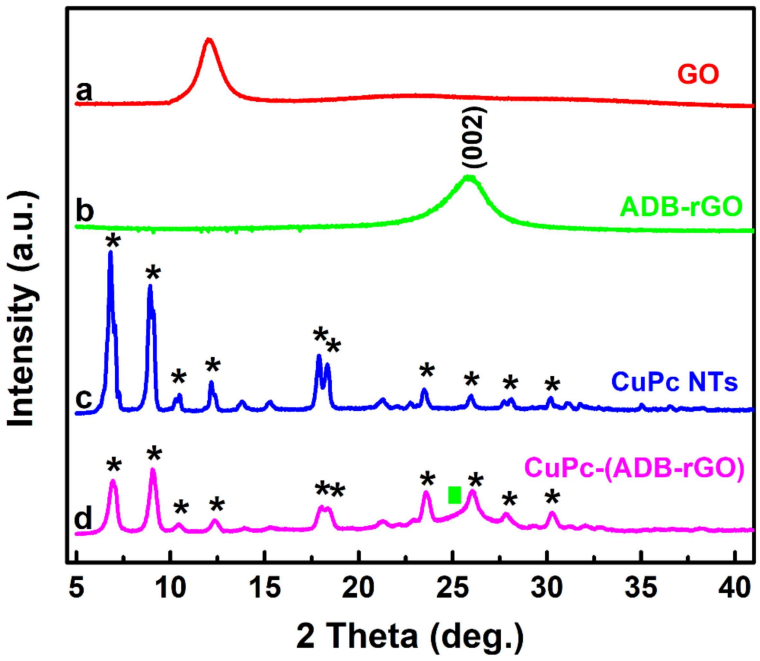


**Fig. 6.7.** XRD images of (a) GO, (b) ADB-rGO, (c) CuPc nanotube and (d) CuPc-(ADB-rGO).

The FTIR spectrum of ADB-rGO shows specific peaks due to C-O-C/B-O-C, C-N, C-OH, C=C, C=O, and $CH_2$ stretching frequencies at 1090, 1120, 1170, 1556, 1632, and 2923 $cm^{-1,}$ respectively (**Fig.6.8**). A broad band around 3410 $cm^{-1}$ may be allocated to N-H and O-H stretching modes [Mukherjee et al. (2017)].

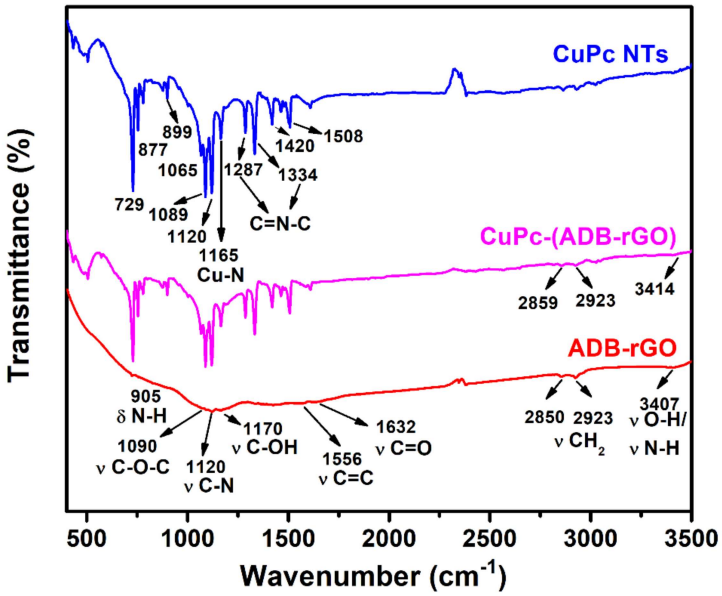


**Fig. 6.8.** FTIR spectra of the synthesized nano additives.

The CuPc nanotubes were characterized by the FTIR spectrum. The pyrrole in-plane modes of the phthalocyanine group are identified as sharp peaks at 899, 1067, 1089, and 1120 $cm^{-1,}$ whereas out of plane modes are seen at 877 $cm^{-1}$ in **Fig.6.8**. The stretching modes of the pyrrole ring are observed at 1420, 1508, and 1609 $cm^{-1}$. The peak at 1165 $cm^{-1}$ is attributed to Cu-N stretching vibration. Moreover, the peaks appearing at 1287 and 1334 $cm^{-1}$ are ascribed to the vibrational mode of π-bridging C=N-C moiety. The spectrum of the

nanohybrid CuPc-(ADB-rGO) reveals the characteristic peaks of CuPc and ADB-rGO [Mukherjee et al. (2017), Samanta et al. (2018)].

The UV-visible spectra of ADB-rGO, CuPc NTs, and CuPc-(ADB-rGO) are depicted **in Fig. 6.9a**. The ADB-rGO shows the characteristic absorption band of rGO at 270 nm [Jha et al. (2012)]. The B (Soret band) and Q bands characteristic of CuPc appear in the ranges 300-450 nm (for $a_{2u}$ π - e.g., π transition) and 600-750 nm (representing $a_{1u}$ π - e.g., π transition) respectively. The splitting observed in the Q band is ascribed to Davydov splitting. There is a redshift in the Q band in CuPc-(ADB-rGO), indicating strong π-π interaction between CuPc NTs and ADB-rGO. The shift towards longer wavelength exhibits concurrence with the charge transfer interaction between the CuPc NTs and ADB-rGO.

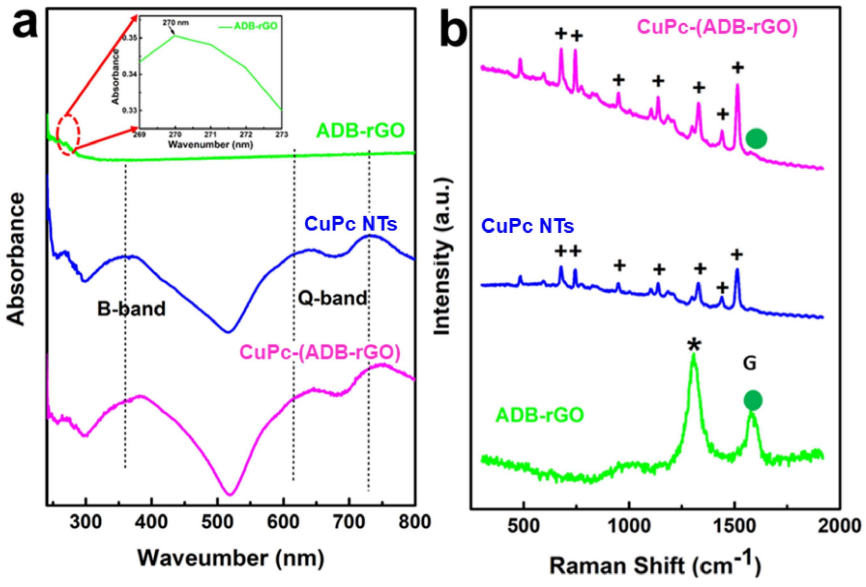


**Fig. 6.9.** (a) UV-vis and (b) Raman spectra of synthesized nanomaterial.

Raman spectra of GO, ADB-rGO, CuPc, and CuPc-(ADB-rGO) are illustrated in **Fig. 6.9b**. The spectrum of GO exhibits distinctive bands G and D at 1346 and 1592 $cm^{-1}$, which correspond to the first-order scattering of $E_{2g}$ phonons of $sp^2$ hybridized carbon atoms and breathing mode of k-point phonons of $A_{1g}$ symmetry respectively [Paul et al. (2019), Mukherjee et al. (2017), Samanta et al. (2018)]. These bands are observed at 1332 and 1590 $cm^{-1,}$ respectively, in the spectrum of ADB-rGO. Raman spectrum of CuPc reveals several peaks at 594, 677, 744, 826, 1010, 1034 and 1101 and 1332 $cm^{-1}$ assignable to $A_{1g}$ of benzene ring deformation, $B_{1g}$ macrocyclic breathing, C-N stretching, isoindole in-plane bending, C-H bending (1034), out of plane C-H bending and stretching vibrations of pyrrole ring respectively [Mukherjee et al. (2017), Samanta et al. (2018)]. The peaks at 1440 and 1515 $cm^{-1}$ correspond to isoindole ring stretching and shift of C-N-C bridge after coordination with $Cu^{2+}$ ion. The characteristic peaks due to $B_{1g}$ and combined modes of $B_{1g}$ and $B_{2g}$ are observable at 1515 and 1440 $cm^{-1}$, respectively. The Raman spectrum of CuPc-(ADB-rGO), however, manifested all the peaks due to CuPc and ADB-rGO. A negative shift of around 10 to 15 $cm^{-1}$ in D and G bands in the case of CuPc-(ADB-rGO) asserts electron transfer type of interaction between CuPc and rGO moieties. Furthermore, a significant hike in the proportion of intensities $I_D/I_G$; GO (0.90), ADB-rGO (1.12), and CuPc-(ADB-rGO) (1.18) is indicative of reduced $sp^2$ domains or increased $sp^3$ character after successive functionalization with ADB and CuPc NTs. Although $-NH_2$ group of ADB attacks covalently at epoxide rings of GO forming -NH-C-C-OH and CuPc NTs interact in a non-covalent fashion. CuPc is efficient enough to bring about Raman enhancement on GO/rGO through

charge-transfer interaction. Possibility of dipole-dipole type of interaction is rare in this case as graphene is a non-polar semiconductor with zero band gap [Ling et al. (2014)].

The XPS survey spectrum of CuPc-(ADB-rGO) denotes the presence of boron, carbon, nitrogen, oxygen, and copper. The chemical states of the above elements have been ascertained by XPS spectra using XPS peak software. The XPS fine spectra of B1s, C1s, N1s, O1s, and Cu2p are displayed in **Fig. 6.10a**. The core-level spectrum of C 1s, **Fig. 6.10b** could be deconvoluted into four peaks with binding energies 284.6, 285.4, 286.5 and 288.9 eV representing carbon in different chemical environments, C-B or C-C/C=C, C-N=C, C-O/C-N, and O-C=O bonds respectively [Jaiswal et al. (2016)]. The correlation of binding energies with different chemical environments is based on the electronegativity of the atoms bonded to carbon. With the increase in electronegativity of the bonded atom, electron density around the carbon atom decreases, consequently the binding energy increases. In CuPc, two types of environments around nitrogen atoms are apparent, namely C-N=C in the phthalocyanine ring and the nitrogen coordinated to the cupric ion. Besides this, borated amine also has a C-N bond. Accordingly, Deconvolution of core-level spectrum of N 1s yielded two peaks at 399.5 and 400.1 eV corresponding to C-N-(H)-C and C-N=C **Fig. 6.10c**. [Jha et al. (2012)]. As evident from the structure of borated amine, boron is directly bonded to both carbon and oxygen. The two peaks with the binding energies 188.5 and 192.1 eV in the high-resolution spectrum of B 1s could be correspondingly ascribed to B-C and B-O bonds in **Fig. 6.10d**. [Jaiswal et al. (2017), Philippon et al. (2011), Spadaro et al. (2018)]. The core-level spectrum

of O 1s exhibits two peaks upon deconvolution, **Fig. 6.10e** with binding energies 531.2 and 532.1 eV [Jaiswal et al. (2017)]. The previous peak could be accorded with C-O bonds of rGO and B-O bond of borated amine while the latter for >C=O of rGO. The XPS fine spectrum of Cu 2p (**Fig. 6.10f)** displays two strong peaks located at 934.2 and 954.3 eV related to the states Cu $2p_{3/2}$ and Cu $2p_{1/2}$, respectively [Jha et al. (2012). The existence of satellite peaks follows the $Cu^{+2}$ state and confirms that its $3dx^2$-$y^2$ orbital is confined to the molecular plane.

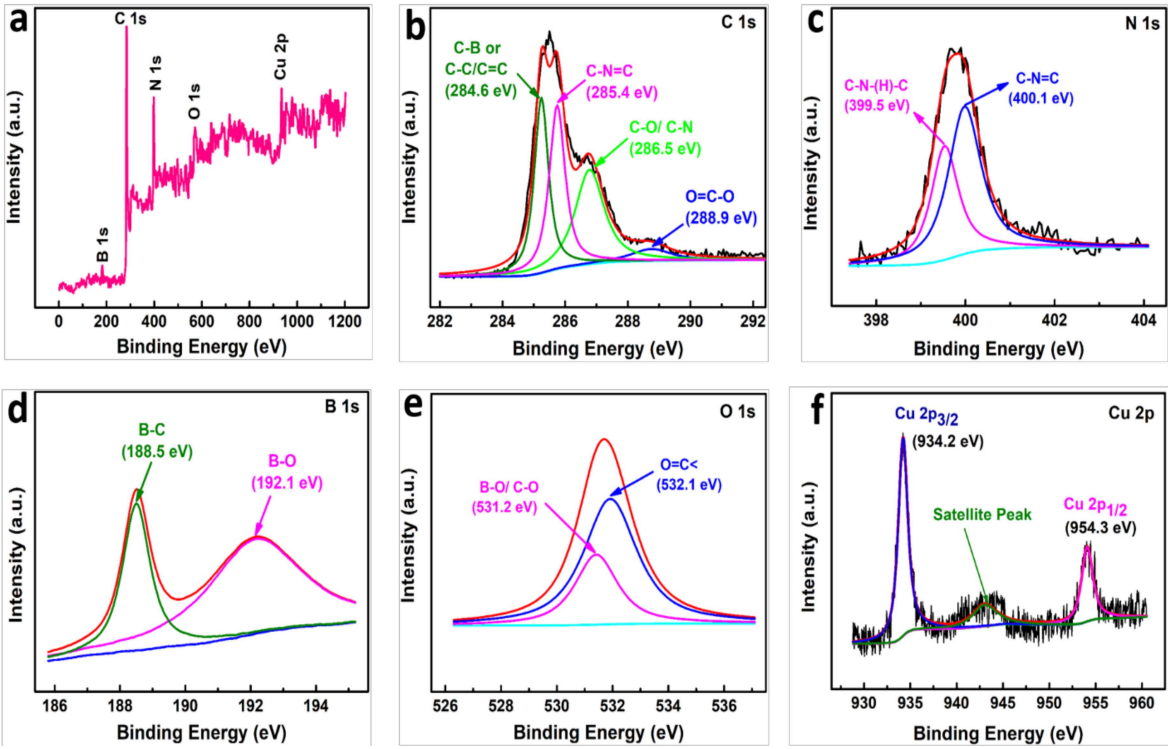


**Fig. 6.10.** XPS spectra of the CuPc-(ADB-rGO) nanomaterial: (a) XPS survey spectra (b) C1s, (c) N 1s, (d) B 1s, (e) O 1s, and (f) Cu 2p spectra.

### 6.4.3. Dispersion Stability of the Blends

The UV/visible spectroscopy was employed to study the dispersion stability of the additives under investigation by measuring their absorbance values in the range 200-800 nm till 48 h at 12h intervals. Since the absorbance measurements require very dilute samples, the optimized concentration of the additive was diluted ten times by PO to prepare test samples. The plots of relative absorbance against settling time for different additives are depicted in **Fig. 6.11a**.

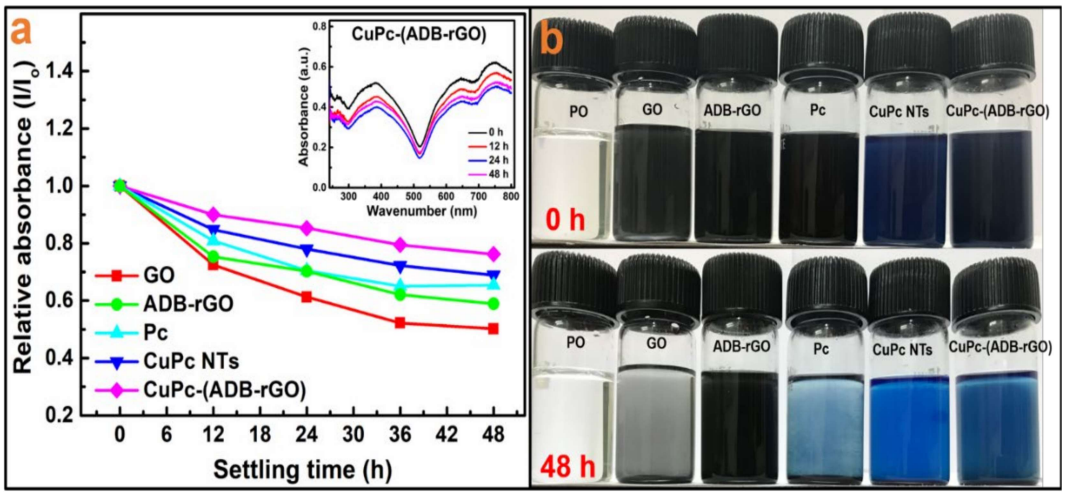


**Fig. 6.11.** (a) Dispersion stability of base oil containing GO, ADB-rGO, Pc, CuPc, and CuPc-(ADB-rGO) studied by UV-vis spectrophotometry [inset showing a decrease in absorbance of CuPc-(ADB-rGO) against time]. (b) Optical photographs of plain PO and PO with different dispersed nano additives at zero time and after 48 hours.

The relative absorbance, as shown in the figure, indicates sufficient stability of all the additives. As apparent from the relative absorbance, the stability of ADB-rGO has

significantly enhanced on the addition of CuPc. Thus, the CuPc-(ADB-rGO) was found to be highly stable as the relative absorbance goes down to 0.80 only. The variation of absorbance for CuPc-(ADB-rGO) within 200-800 nm for 48 h at every 12 h from the beginning is shown in the inset. From **Fig. 6.11b,** it can be noted that the composite shows a minute reduction in absorbance of B and Q bands of CuPc within the stipulated period, 48 h.

### 6.4.4. Evaluation of Tribological Properties

The observed MWD are shown in **Fig. 6.12a** for plain paraffin oil in the absence and the presence of CuPc nanotubes and CuPc-(ADB-rGO) at different concentrations starting from 0.025 to 0.15% w/v under ASTM D 4172 test conditions. Although the additives appear to be active at all the concentrations, the best results for CuPc were obtained at 0.10% w/v while for composite at 0.05 % w/v. Thus, 0.05% w/v was considered as the optimized concentration.

The wear abatement test of base oil with and without different additives was carried out following the norms imposed by American Society for Testing and Materials, ASTM D4172. The observed data for mean wear scar diameter (MWD) and the average coefficient of friction (COF) is presented in **Fig. 6.12b** as a bar diagram. The MWD, in the presence of paraffin oil (0.733), encounters a higher reduction in the case of CuPc (39.15%) as compared to just Pc (26.33). The reductions in MWD in the presence of GO (9.95%) also increase when

it is functionalized, ADB-rGO (17.87%). However, a remarkable reduction in MWD (55.66%) is observed when the admixture of CuPc-(ADB-rGO) is used.

Further, the average coefficient of friction for paraffin oil was observed as 0.0756, which is very well within the limits of boundary lubrication. The value of COF reduces further in the presence of the additives; Pc (28.83%), CuPc (41.80), GO (2.12%), ADB-rGO (15.61%), and severe diminution in case of CuPc-(ADB-rGO) (50.80%). The large magnitude of reduction in COF indicates increased adsorption of the additive on the ball surface. It may be tentatively stated that the lubrication state after the addition of additives remains under the boundary lubrication regime.

The enhancement in % reduction of MWD and COF from Pc to CuPc nanotubes is in tune with the results of molecular dynamics, particularly RDF plots. The complexation of Pc to form CuPc nanotubes has exalted the tribological activity. The covalent functionalization of GO by ADB has resulted in a severe reduction of MWD and COF, thus increasing the activity. Maximum reduction in wear and friction is noticeable for CuPc-(ADB-rGO), emphasizing synergic behavior.

Deviation of COF of proximal surfaces against time at an applied load of 392 N in plain oil and its blends with the tested additives is depicted in **Fig. 6.12c**. Initially, the performance is almost similar for all the additives because of the absence of tribofilm. Formation of tribofilm.is indeed, time-dependent. With an increase of time, tribochemical reactions start eventually forming a tribofilm. The nature of tribofilm is vital in interpreting the antifriction

and antiwear efficiencies of the additives. Ostensibly, the trend in COF values for all the additives conforms with the antiwear data. Undoubtedly, the most effective and persistent tribofilm is formed in the case of CuPc-(ADB-rGO) as it shows the lowest value of COF.

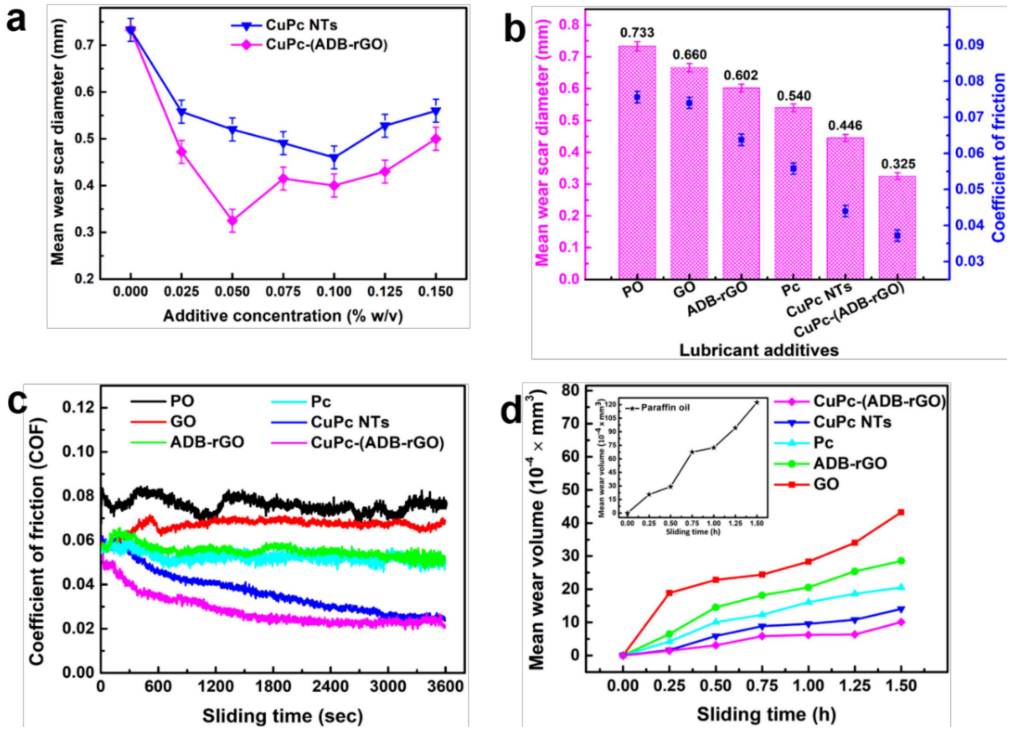


**Fig. 6.12. (a)** Optimization of concentration of different additives and Variation of tribological parameters of paraffin oil with and without optimized concentration (0.05% w/v) of different additives under ASTM D4172 conditions **(b)** mean wear scar diameter **(c)** coefficient of friction as a function of sliding time **(d)** mean wear volume with sliding time for 1.5 h test duration.

Further, the average coefficient of friction for paraffin oil was observed as 0.0756, which is very well within the limits of boundary lubrication. The value of COF reduces further in the presence of our additives, indicating increased adsorption of the additive. EDX/ XPS/ AFM

studies of the wear scar also show strong adsorption of the additive. It may be tentatively stated that the lubrication state after the addition of additives remains under the boundary lubrication regime.

The antiwear test was performed at 392 N for 1.5 h, and at 15 min interval, corresponding values of MWD were observed. For wear rate determination, mean wear volume (MWV) is considered to be more appropriate than mean wear scar diameter (MWD). The MWV data have been calculated from MWD values using Archard wear equation [Kumar et al. (2002)] (given in Chapter 2). Alteration of MWV against sliding time was plotted and displayed in **Fig. 6.12d**.

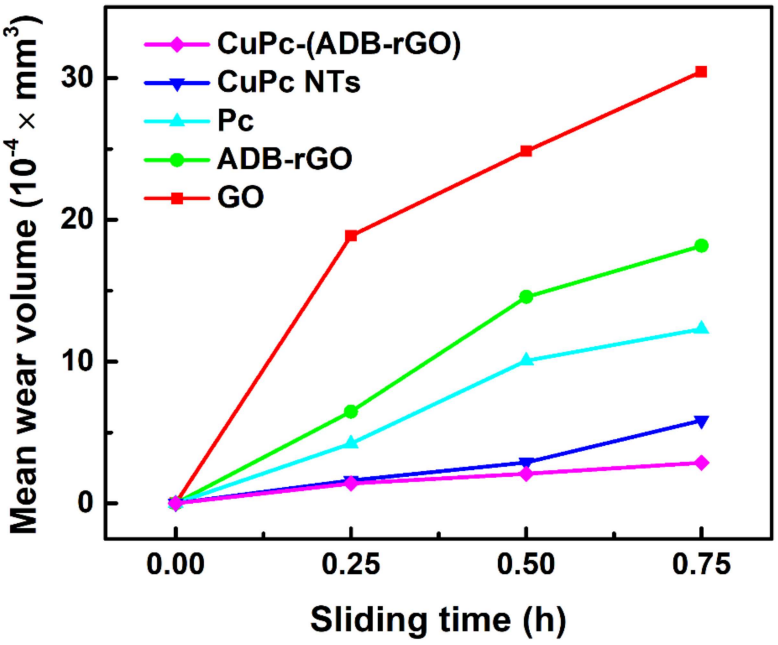


**Fig. 6.13.** Determination of running-in wear rate by varying mean wear volume with time (h) for paraffin oil containing (0.05% w/v) nano additives at 392 N applied load.

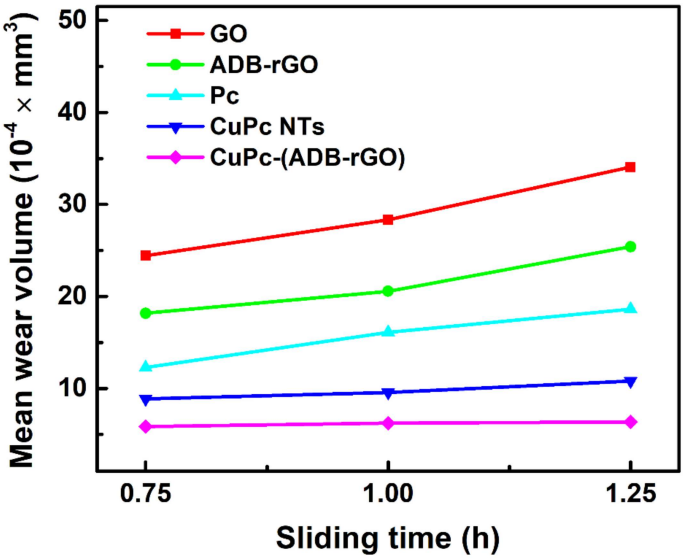


**Fig. 6.14.** Determination of steady-state wear rate by varying mean wear volume with time (h) for paraffin oil containing (0.05% w/v) nano additives at 392 N applied load.

A linear regression model was fitted to obtain wear rate [Jaiswal et al. (2016), Verma et al. (2019), Kumar et al. (2002)]. Up to 0.75 h, the running-in period was considered, and beyond that, it was the steady-state period [Verma et al. (2020)]. Accordingly, running-in and steady-state wear rates were calculated and are summarized in **Table 6.2**, and the concerned figures are illustrated in **Fig. 6.13** and **6.14.** The wear rate data given in **Table 6.2** comply with the antiwear efficiency of the additives.

As expected, huge values of running-in ($84\times10^{-4}$ $mm^3/h$) and steady-state wear rate ($53\times10^{-4}$ $mm^3/h$) were observed for blank oil. On the other hand, remarkable diminution was noted for respective wear rates ($10^{-4}$ $mm^3/h$) when its admixtures with different additives were taken; GO (39,19), ADB-rGO (25,14), Pc (17,13), CuPc NTs (8,4), and CuPc-(ADB-

rGO) (4,1). Magnitudes of their wear rates corroborate the antiwear properties of the admixtures. Thus, the suitability of CuPc-(ADB-rGO) as an illustrious tribo-active additive may be adjudged by a massive reduction in running-in and steady-state wear rates, 95.24%, and 98.11%, respectively.

The running-in wear rate is inherently higher than the steady-state wear rate because in the beginning, the frictional forces are high, and various molecular level adjustments are to be incorporated. For the safety of a machine, the steady-state wear rate has to be minimized. Its value for CuPc-(ADB-rGO) supports the highest antiwear efficiency.

**Table 6.2.** Wear-rate for paraffin oil (PO) in the presence and absence of different additives

| S/N | Lubricants | Wear rate ($10^{-4}$ × $mm^3$/h) | |
|---|---|---|---|
| | | Running-in | Steady-state |
| 1 | PO | 84 | 53 |
| 2 | GO | 39 | 19 |
| 3 | ADB-rGO | 25 | 14 |
| 4 | Pc | 17 | 13 |
| 5 | CuPc NTs | 8 | 4 |
| 6 | CuPc-(ADB-rGO) | 4 | 1 |

The load ramp test was carried out following ASTM D 5183 conditions: 392 N load, 600 rpm, 75°C temperature, at 0.05% w/v concentration of the additives for 60 min. After that, the load was added in increments of 98 N at 10 min interval, and frictional torque was noted.

**Fig. 6.15** illustrates the variation of frictional torque against the load. As evident from the figure, seizure of the mating surfaces occurs at 1078 N when paraffin oil alone is used. However, the seizure load increases in the presence of its blends except GO (980 N), ADB-rGO (2548 N), Pc (2058 N), CuPc NTs (2842 N), and CuPc-(ADB-rGO) (3136 N). Thus, it can be interpreted that the tribofilm formed in the case of CuPc-(ADB-rGO) is strong enough to support the heavy load up to 3136 N.

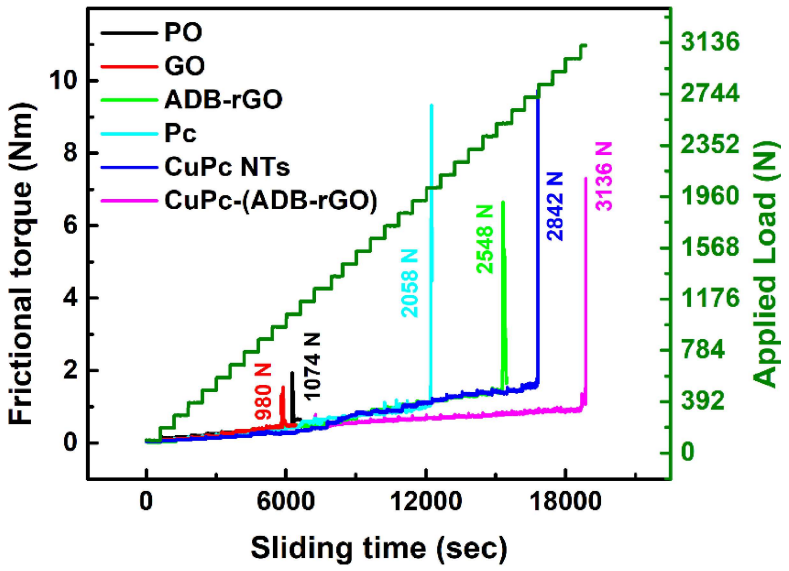


**Fig. 6.15.** Variation of frictional torque as a function of stepwise loading and time for PO in absence and presence of different additives: sliding speed, 600 rpm; temperature, 75 °C; concentration of additives, 0.05% w/v.

### 6.4.5. Morphology of the Wear Track

The SEM and AFM techniques were adopted to study the morphological characteristics of the tribo surface after the antiwear test. The SEM images of the plain lube in the absence and

the presence of investigated nano additives are presented in **Fig. 6.16**. The wear scar surface is highly rumpled when the blank lubricant is used. On the other hand, the presence of its blends makes the surface much leveled. The leveling of the surfaces conforms to the antiwear efficacy of the investigated additives. The inset in all the micrographs reveals the values of MWD too. The MWD data is obviously in accordance with antiwear properties; paraffin oil (0.733 mm), GO (0.660 mm), ADB-rGO (0.602 mm), Pc (0.540 mm), CuPc NTs (0.446 mm) and CuPc-(ADB-rGO) (0.325 mm ).

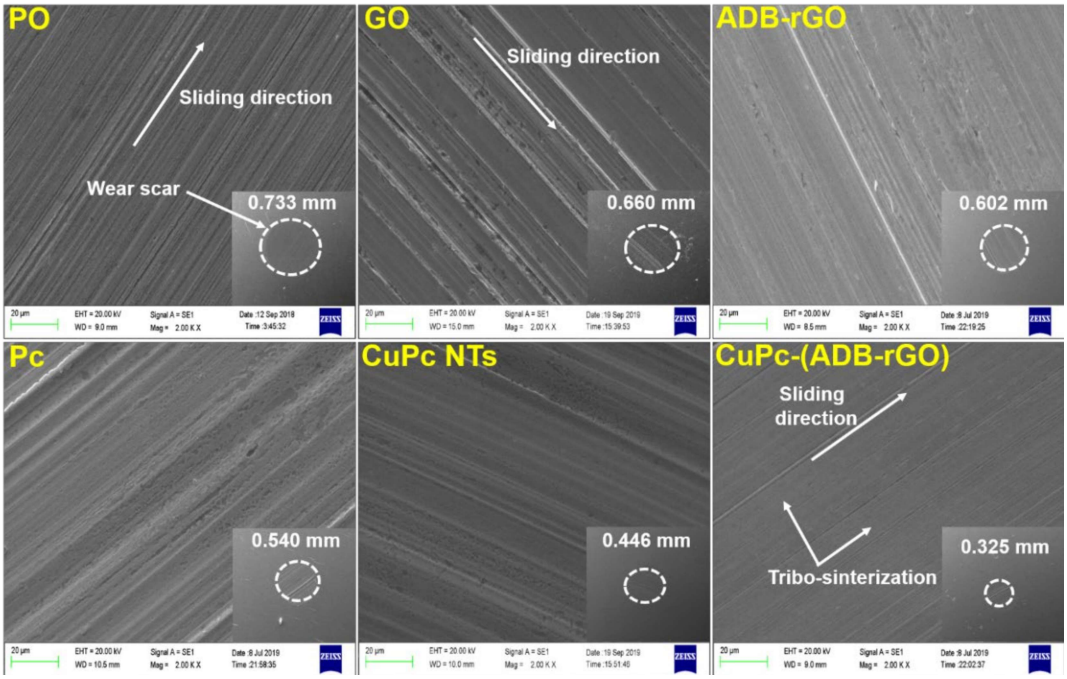


**Fig. 6.16.** SEM micrographs (inset: full view of wear scar at 100X, wear scar surface at 2.00KX magnification) of the worn steel surface lubricated with paraffin oil with and without different nano additives (0.05% w/v) after the antiwear test.

The AFM images (*3D)* of the worn surface developed after the antiwear test of base oil with or without additives are portrayed in **Fig. 6.17**. The surface roughness in terms of area (Sq) and line roughness (Rq) is given with the images. Visibly, the roughness has decreased with an increase in antiwear properties of the additives.

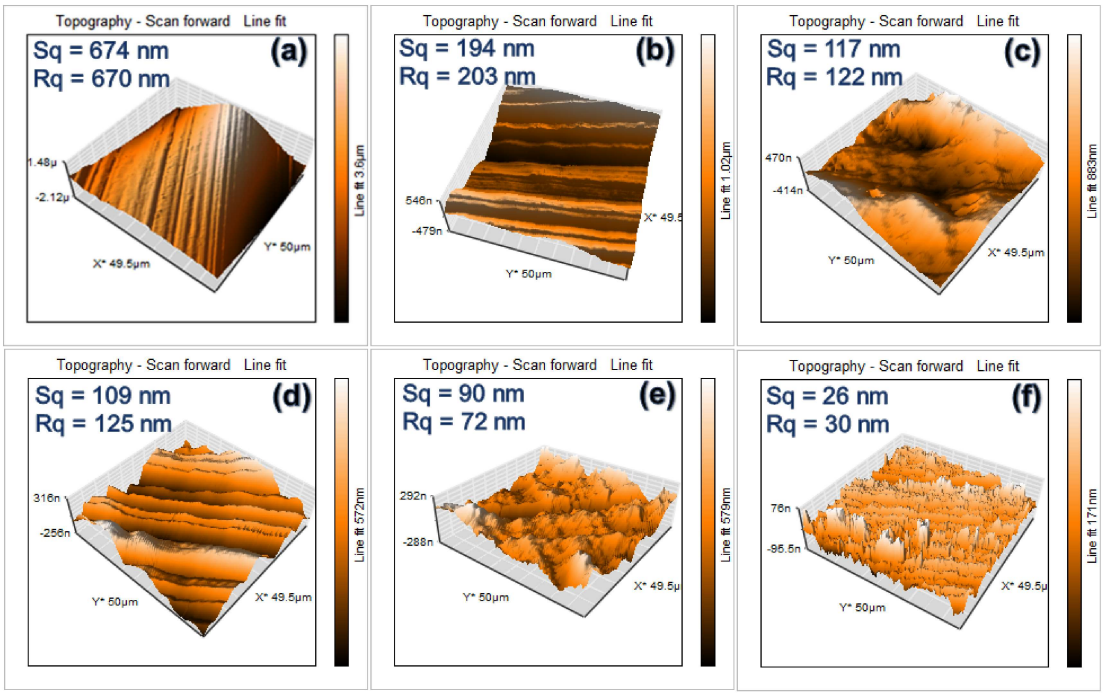


**Fig. 6.17.** Three-dimensional (3D) AFM images of the worn steel surface lubricated with different additives (0.05% w/v) in paraffin oil after antiwear test: (a) PO, (b) GO, (c) ADB-rGO, (d) Pc, (e) CuPc NTs, and (f) CuPc-(ADB-rGO).

### 6.4.6. Characterization of Tribofilm

The EDX spectrum of the worn surface after ASTM D4172 test using paraffin oil and the admixture containing CuPc-(ADB-rGO) are shown in **Fig. 6.18a** and **Fig. 6.18b,**

respectively. **Fig. 6.18b** reveals the presence of additional elements copper and nitrogen confirming the adsorption of the additive on steel surface (however, boron could not be detected, probably due to its small size). These elements have acted positively towards strengthening the tribofilm.

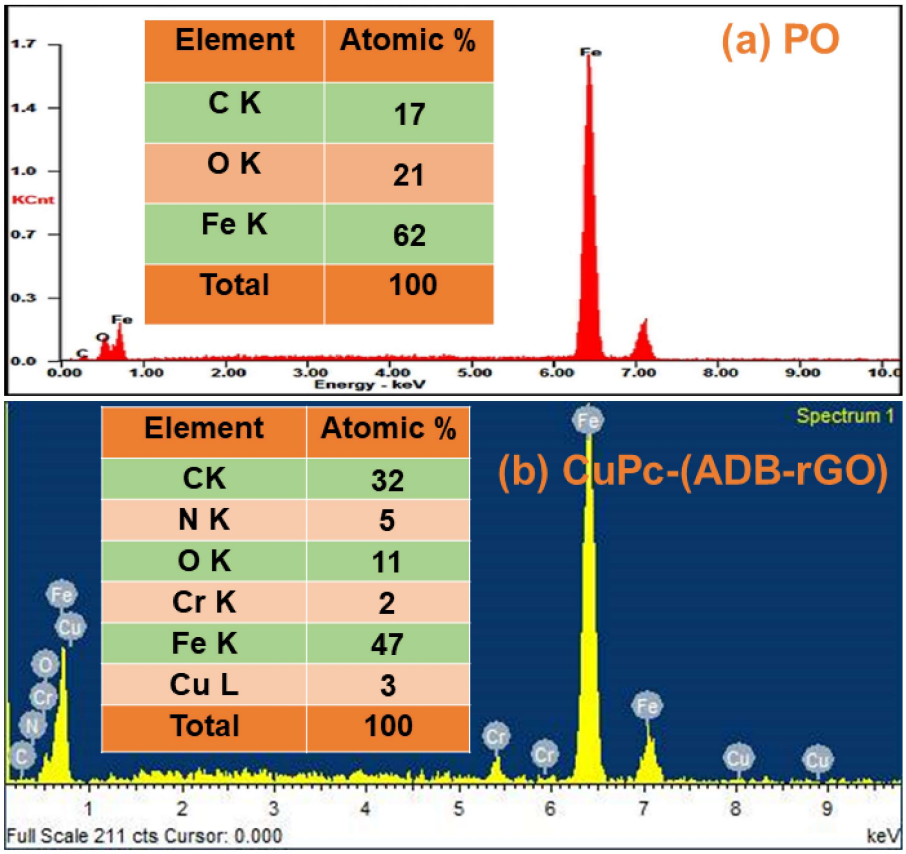


**Fig. 6.18.** EDX spectra of worn surface lubricated with (a) Blank PO and (b) 0.05% w/v of CuPc-(ADB-rGO) after ASTM D4172 test.

The composition of tribofilm in the presence of the additive CuPc-(ADB-rGO) was further studied by the XPS spectra of the worn surface after the ASTM D 4172 test. The

chemical states of constituent elements of CuPc-(ADB-rGO) could be inferred from XPS spectra by XPS peak software. The deconvoluted XPS core spectra of B1s, C1s, N1s, O1s, and Cu2p and Fe2p are shown in **Fig. 6.19.** The core-level spectrum of C 1s, **Fig. 6.19a,** shows four peaks with binding energies 283.4, 284.2, 285 and 287.2 eV representing carbon in different chemical environments, C-B/C-C, C=C, C-N=C and C=O bonds respectively [Jaiswal et al. (2014), Jaiswal et al. (2016)]. The correlation of binding energies with different chemical environments is based on the electronegativity of the atoms bonded to carbon. With the increase in electronegativity of the bonded atom, electron density around the carbon atom decreases, consequently the binding energy increases. Deconvolution of core-level spectrum of N 1s yielded two peaks at 398.1 and 400.2 eV corresponding to BN and C-N=C, **Fig 6.19b**.[Jaiswal et al. (2014), Jaiswal et al. (2016)]. In **Fig. 6.19c,** the two peaks with the binding energies 191.3 and 192.0 eV in the high-resolution spectrum of B 1s could be ascribed to boron nitride (BN) and $B_2O_3$ respectively [Jaiswal et al. (2014), Jaiswal et al. (2016)]. The core-level spectrum of O 1s exhibits peaks, **Fig. 6.19d** with binding energy 529.8 and 532.2 eV, which could be accorded with $B_2O_3$ and >C=O bonds of rGO. Besides, one more peak is observed having binding energy 530.9 eV, which corresponded to *in situ* formed $Fe_2O_3$/ CuO respectively [Jaiswal et al. (2014), Jaiswal et al. (2016)]. The oxidation state of copper remains unchanged in the tribofilm as evidenced by the presence of peaks at 934.4 and 954.4 eV for Cu $2p_{3/2}$ and Cu $2p_{1/2}$, respectively, in **Fig. 5619e** [Jha et al. (2013)]. The binding energies of Fe $2p_{3/2}$ at 711.7 eV and $2p_{1/2}$ at 725.2 eV (**Fig.6.19f)** together

indicate the presence of iron oxide $Fe_2O_3$, confirming the oxidation of steel surface iron during the rubbing process [Verma et al. (2019)].

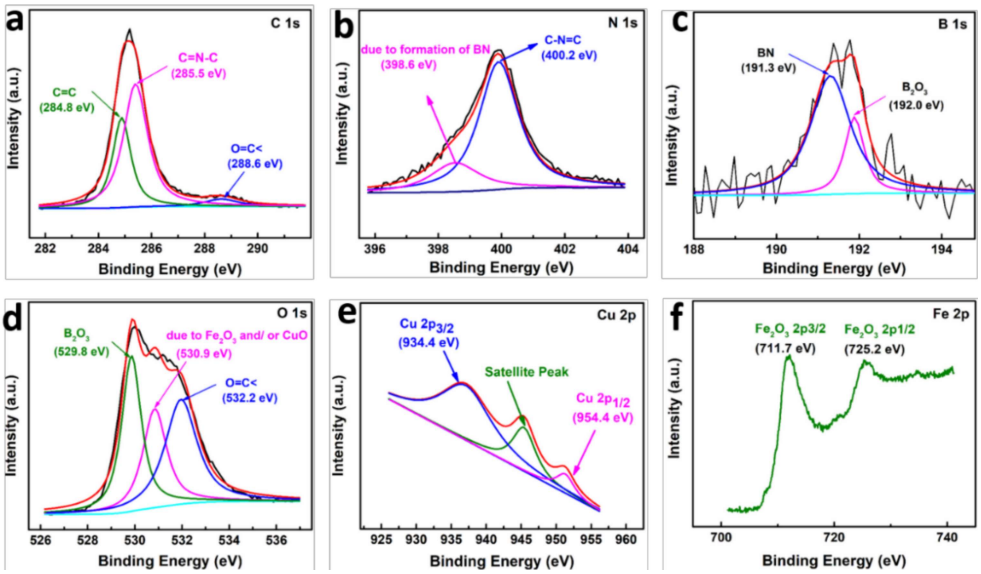


**Fig. 6.19.** XPS spectra of the worn surface lubricated with CuPc-(ADB-rGO) nanomaterial: (a) C 1s, (b) N 1s, (c) B 1s, (d) O 1s, (e) Cu 2p, and (f) Fe 2p spectra.

### 6.4.7. Mechanism of Tribo-Interaction of Additives

From the results and discussion, it can be cogently stated that the additive is primarily adsorbed on the mating surfaces through hetero-atoms and π-electrons, leading to the formation of tribofilm under test conditions. The *in situ* formed tribofilm supports the applied load. The nature of tribofilm is undoubtedly imperative for the interpretation of the difference in antiwear efficacy of the studied additives. The covalent interaction of ADB with GO through nucleophilic substitution at the epoxide ring has exalted the efficiency of the

otherwise tribo-active GO/rGO. The increase in efficiency may be attributed to improved dispersibility in the base lube and enhanced adhesion on the steel surface. Besides, a strong synergy between electron-deficient boron and electron-rich nitrogen has yielded *in situ* formed of boron nitride (BN), another tribo-active material at the interface. The exquisite efficiency of CuPc-(ADB-rGO) may be plausibly explained by the non-covalent interaction of CuPc NTs by its π electrons/van der Waals forces with ADB-rGO. The CuPc itself is an exemplary antiwear additive owing to its layered structure. The layered structures invariably are known to facilitate lubrication by decreasing the shearing force. The two materials with layered structure rGO and CuPc are further supported by the third layered material formed *in situ*, boron nitride (BN), as evidenced from XPS spectra of the tribofilm. Under tribo test conditions ADB, an organic compound decomposes. Since synergy between electron-rich nitrogen (due to lone pair) and electron-deficient boron is very well established [Jaiswal et al. (2014), Li et al. (2014), Qiao et al. (2003)], they combine to give BN, a ceramic material stable under extreme conditions. The *in-situ* formed BN at the interface therefore affects the lubricating behavior effectively.

The cumulative effect of the three, CuPc, rGO, and boron nitride, has resulted in incredible tribo-activity of CuPc-(ADB-rGO). In addition to this, a boron-iron glassy network formed by the intake of iron oxide ($Fe_2O_3$) into $B_2O_3$ during tribochemical reaction also helps in lubrication [Jaiswal et al. (2017), Philippon et al. (2011), Spadaro et al. (2018)]. Thus, the developed tribofilm is so robust, tenacious, and durable that it can bear the load up to 3136N.

## 6.5. Conclusions

To improve lubricating behavior of graphene oxide, its covalent functionalization was implemented as a tool. 2-Amino diphenyl borate (ADB) was selected explicitly to functionalize GO for availing the advantage of B-N synergy during tribo test, causing *in situ* formation of boron nitride. The ADB has attacked at epoxide rings of GO by nucleophilic -$NH_2$ group and GO reduced finally to rGO. For the furtherance of tribo-activity of ADB-rGO, tribo-active phthalocyanine (Pc) and the copper (II) complex (CuPc) were considered. Molecular dynamics studies for adsorption of Pc and CuPc on the steel surface in paraffin oil revealed that CuPc shows a higher affinity for adsorption on the iron slab because of the strong Fe-Cu linkage and thus exhibits a relatively higher tribological efficacy and lower wear rate compared to Pc. Accordingly, CuPc was favored over Pc. Since the CuPc tends to fold and unfold the structure, its nanotubes (NTs) were prepared, characterized, and used for non-covalent functionalization of ADB-rGO to yield CuPc-(ADB-rGO).

All the additives were characterized by XRD and spectroscopic techniques; FTIR, UV/visible, and specifically XPS was also used for CuPc-(ADB-rGO). The techniques HR-SEM, TEM, HR-TEM were employed for morphological studies. The tribological activity of Pc, CuPc nanotubes, ADB-rGO, and CuPc-(ADB-rGO), was assessed by ASTM D4172 and ASTM D5183 standards in paraffin oil. The relative order of tribological activity was obtained as:

CuPc-(ADB-rGO) > CuPc NTs > Pc > ADB-rGO > GO > PO

The activity of CuPc nanotubes was greater than that of Pc as the former is a layered structure, which increases the feasibility of lubrication. The ADB-rGO performed much better than GO due to covalent functionalization, increased adhesion on steel surface, enhanced dispersibility, and additionally favored boron and nitrogen interaction under test conditions due to strong synergy. Upon modification of GO by covalent and non-covalent functionalizations, antiwear/antifriction efficiencies and load-carrying ability have categorically advanced with minimized wear rates. Besides, the functionalizations have led to the enhancement of the structural stability of graphene by preventing agglomeration and restacking, the feasibility of its dispersion in the desired media, and adhesion of GO to the steel surface. Since the layered structure of additives with weak Van der Waals forces between adjacent layers facilitate lubrication, the illustrious activity of CuPc-(ADB-rGO) is attributed to the accretive effect of layered structures of CuPc, rGO and BN formed *in situ*. Besides, a boron-iron glassy network [Philippon et al. (2011)] formed during tribochemical reaction also cooperated in the enhancement of lubrication.